1 **Shotgun scanning glycomutagenesis: a simple and efficient strategy for**

2 **constructing and characterizing neoglycoproteins**

3

4 Mingji Li[1†], Xiaolu Zheng[1†], Sudhanshu Shanker[2], Thapakorn Jaroentomeechai[1], Tyler D.

5 Moeller[1], Sophia W. Hulbert[3], Ilkay Koçer[1], Josef Byrne[1], Emily C. Cox[4], Qin Fu[5], Sheng

6 Zhang[5], Jason W. Labonte[2,6], Jeffrey J. Gray[2]* and Matthew P. DeLisa[1,3,4,5]*

7

8 [1]Robert F. Smith School of Chemical and Biomolecular Engineering, Cornell University,

9 Ithaca, NY 14853 USA

10 [2]Department of Chemical and Biomolecular Engineering, Johns Hopkins University,

11 Baltimore, MD 21218 USA

12 [3]Biochemistry, Molecular and Cell Biology, Cornell University, Ithaca, NY 14853 USA

13 [4]Biomedical and Biological Sciences, College of Veterinary Medicine, Cornell University,

14 Ithaca, NY 14853 USA

15 [5]Cornell Institute of Biotechnology, Cornell University, Ithaca, NY 14853 USA

16 [6]Department of Chemistry, Franklin & Marshall College, Lancaster, PA 17604 USA

17

18 *Address correspondence to: (1) Matthew P. DeLisa, Robert Frederick Smith School of

19 Chemical and Biomolecular Engineering, Cornell University, Ithaca, NY 14853 USA. Tel:

20 607-254-8560; Email: md255@cornell.edu; and (2) Jeffrey J. Gray, Department of

21 Chemical and Biomolecular Engineering, Johns Hopkins University, Baltimore, MD 21218

22 USA. Tel: 410-516-5313; Email: jgray@jhu.edu.

23

24 [†]These authors contributed equally to this work.

25

26 **Significance**

27 Asparagine-linked (*N*-linked) protein glycosylation–the covalent attachment of complex

28 sugars to the nitrogen atom in asparagine side-chains–is the most widespread

29 posttranslational modification to proteins and also the most complex. *N*-glycosylation

30 affects a significant number of cellular proteins and can have profound effects on their

31 most important attributes such as biological activity, chemical solubility, folding and

1   stability, immunogenicity, and serum half-life. Accordingly, the strategic installation of

2   glycans at naïve sites has become an attractive means for endowing proteins with

3   advantageous biological and/or biophysical properties. Here, we describe a glycoprotein

4   engineering strategy that enables systematic investigation of the structural and functional

5   consequences of glycan installation at every position along a protein backbone and

6   provides a new route to bespoke glycoproteins.

7

8   **Abstract**

9   As a common protein modification, asparagine-linked (*N*-linked) glycosylation has the

10   capacity to greatly influence the biological and biophysical properties of proteins.

11   However, the routine use of glycosylation at naïve sites as a strategy for engineering

12   proteins with advantageous properties is currently limited by our inability to construct large

13   collections of glycoproteins for interrogating the structural and functional consequences

14   of glycan installation. To address this challenge, we describe a combinatorial strategy

15   termed shotgun scanning glycomutagenesis (SSGM) in which DNA libraries encoding all

16   possible glycosylation site variants of a given protein are constructed and subsequently

17   expressed in glycosylation-competent bacteria, thereby enabling rapid determination of

18   glycosylatable sites in the protein. Moreover, the resulting neoglycoproteins can be

19   readily subjected to available medium- to high-throughput assays, making it possible to

20   systematically investigate the structural and functional consequences of glycan

21   conjugation along a protein backbone. The utility of this approach was demonstrated with

22   three different acceptor proteins, namely bacterial immunity protein Im7, bovine

23   pancreatic ribonuclease A, and a human anti-HER2 single-chain Fv antibody, all of which

24   were found to tolerate *N*-glycan attachment at a large number of positions and with

25   relatively high efficiency. The stability and activity of many glycovariants was measurably

26   altered by the *N*-linked glycan in a manner that critically depended on the precise location

27   of the modification. Importantly, we anticipate that our workflow for creating and

28   characterizing large ensembles of neoglycoproteins should provide access to unexplored

29   regions of glycoprotein structural space and to custom-made glycoproteins with desirable

30   properties.

31

1   Introduction

2   Glycosylation of asparagine residues is one of the most abundant and structurally

3   complex protein post-translational modifications (1, 2) and occurs in all domains of life

4   (3). Owing to their relatively large size and hydrophilicity or simply their presence at

5   definite locations, asparagine-linked (*N*-linked) glycans can significantly alter protein

6   properties including biological activity, chemical solubility, folding and stability,

7   immunogenicity, and serum half-life (4, 5). Hence, glycosylation effectively increases the

8   diversity of the proteome by enriching the repertoire of protein characteristics beyond that

9   dictated by the twenty canonical amino acids. For example, accumulating evidence

10   indicates that the immune system diversifies the repertoire of antigen specificities by

11   exclusively targeting the antigen-binding sites of immunoglobulins (IgGs) with post-

12   translational modifications, in particular *N*-linked glycosylation (6). Moreover, the profound

13   effect of glycans on proteins has prompted widespread glycoengineering efforts to

14   rationally manipulate key glycosylation parameters (*e.g.*, glycan size and structural

15   composition, glycosite location and occupancy) as a means to optimize protein traits for

16   a range of different industrial and therapeutic applications (7-10).

17   Despite some notable successes, the routine use of glycosylation as a strategy for

18   engineering proteins with advantageous properties is currently limited by our inability to

19   predict which sites within a protein are glycosylatable and how glycosylation at permissive

20   sites will affect protein structure and function. Indeed, a deeper understanding of the

21   design rules (*i.e.*, how glycans influence the biological and biophysical properties of a

22   protein) represents a grand challenge for the glycoprotein engineering field. To this end,

23   computational approaches have enabled *in silico* exploration of glycosylation-induced

24   effects on protein folding and stability (11, 12); however, these involve a trade-off between

25   molecular detail and glycoprotein size, with full-atomistic molecular dynamics simulations

26   typically limited to only short glycopeptides or protein domains (11). To experimentally

27   probe the consequences of glycosylation ideally requires access to large collections of

28   chemically defined glycoproteins in sufficient quantities for characterization (13).

29   Mammalian cells represent an obvious choice to source proteins with both natural and

30   naïve glycosites; however, studies using mammalian cell-based expression systems

31   typically involve only a small number of designs (~15 or fewer) (14-17) presumably

3

1   because of the time-consuming, low-throughput nature of gene transfection and culturing

2   of mammalian cells. In addition, the intrinsic variability with respect to the glycan structure

3   at a given site (microheterogeneity) can be unpredictable and difficult to control in

4   mammalian expression systems. Another option is chemical synthesis, which can furnish

5   structurally uniform glycopeptides for investigating the local effects of *N*-linked glycans on

6   peptide conformation (18). While this approach is not amenable to full-length proteins,

7   advances in expressed protein ligation (EPL) have opened the door to convergent

8   assembly of chemically synthesized glycopeptides with recombinantly expressed protein

9   domains to form larger glycoproteins bearing complex *N*-glycans installed at discrete sites

10 (19). Using this technology, Imperiali and colleagues created a panel of seven site-

11 specifically glycosylated variants of the bacterial immunity protein Im7 modified with the

12 disaccharide *N,N'*-diacetylchitobiose (GlcNAc$_2$) and assessed the kinetic and

13 thermodynamic consequences of glycan installation at defined locations (20).

14 Unfortunately, EPL is a technically demanding procedure, requiring manual construction

15 of each individual glycoprotein, which effectively limits the number of testable glycosite

16 designs to just a small handful.

17   To move beyond these "one-glycosite-at-a-time" methods for supplying

18 glycoproteins, herein we describe a scalable technique called <u>s</u>hotgun <u>s</u>canning

19 <u>g</u>lyco<u>m</u>utagenesis (SSGM) that involves design and construction of combinatorial

20 acceptor protein libraries in which: (i) each member of the library carries a single *N*-

21 glycosite "mutation" introduced at a defined position along the protein backbone; and (ii)

22 the complete ensemble of glycan acceptor sites (sequons) in the library effectively covers

23 every possible position in the target protein (**Fig. 1**). The resulting SSGM libraries are

24 expressed using *N*-glycosylation-competent bacteria in the context of glycoSNAP

25 (<u>glyco</u>sylation of <u>s</u>ecreted <u>N</u>-linked <u>a</u>cceptor <u>p</u>roteins), a versatile high-throughput screen

26 based on extracellular secretion of glycosylated proteins (21). Using this new glycoprotein

27 engineering tool, we constructed and screened SSGM libraries corresponding to three

28 model proteins: bacterial immunity protein Im7, bovine pancreatic ribonuclease A (RNase

29 A), and a human single-chain variable fragment antibody specific for HER2 (scFv-HER2).

30 Our results revealed that installation of *N*-glycans was tolerated at a large number of

31 positions and in all types of secondary structure, with relatively high *N*-glycosylation

4

1   efficiency in the majority of cases. For many of these glycoproteins, the presence of *N*-

2   glycans at naïve sites had a measurable effect on protein stability and/or activity in a

3   manner that depended on the precise location of the modification. Taken together, these

4   findings demonstrate the ability of the SSGM method to yield large collections of

5   discretely modified neoglycoproteins that collectively reveal glycosylatable sites and

6   provide insight on the influence that site-specific *N*-glycan installation has on structural

7   and/or functional properties.
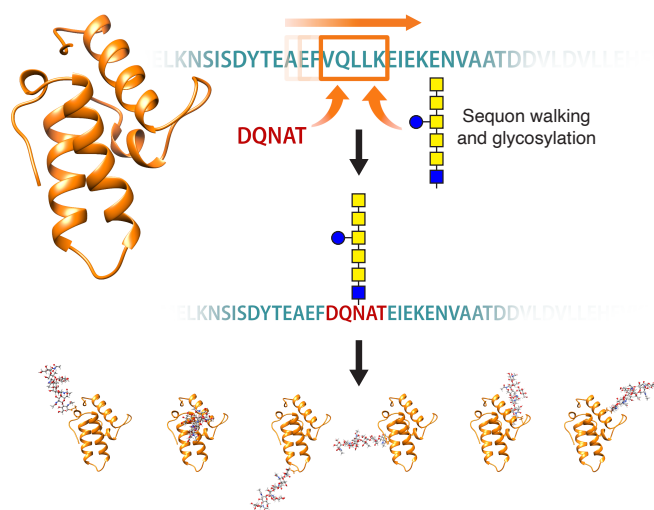
8

9   **Figure 1. Constructing neoglycoproteins by shotgun scanning glycomutagenesis (SSGM).**
10   Schematic of SSGM, a glycoprotein engineering method based on combinatorial protein libraries in which
11   glycosylation "sequon walking" is used to introduce an acceptor site at every possible position along a
12   protein backbone. Note that the multi-residue nature of a sequon (*e.g.*, N-X-S/T or D/E-X_1-N-X_2-S/T where
13   X, X_1, $X_2 \neq$ P) necessitates insertion or replacement of up to five additional amino acid substitutions at each
14   position. The resulting library is expressed in glycoengineered bacteria, providing an opportunity for each
15   library member to be expressed and glycosylated in a manner that is compatible with high-throughput
16   screening via glycoSNAP to interrogate the glycosylation phenotype of individual variants. By integrating
17   expressed SSGM libraries with multiplexable assays, the biochemical and biophysical properties of each
18   neoglycoprotein can be individually interrogated.
19

20   **Results**

21   **Reliable detection of acceptor protein glycosylation by glycoSNAP screening.** To

22   enable screening of SSGM libraries, we first sought to adapt glycoSNAP screening for

23   proteins of interest (POIs). In the original glycoSNAP assay, we genetically modified

24   *Escherichia coli* YebF, a small (10 kDa in its mature form) extracellularly secreted protein

25   (22), with an artificial glycosite (*e.g.*, N-X-S/T or D/E-X_1-N-X_2-S/T where X, X_1, $X_2 \neq$ P) at

26   its C-terminus. The modified YebF protein was expressed in *E. coli* cells carrying the

27   *Campylobacter jejuni N*-glycosylation machinery (23) that were bound to a nitrocellulose

1   filter membrane. Following secretion out of filter-bound colonies, putatively glycosylated

2   YebF was captured on a second nitrocellulose membrane, which was probed with

3   antibodies or lectins to detect *N*-linked glycans. In this way, glycoSNAP creates a

4   convenient genotype–glycophenotype linkage for facile scoring (glycosylated versus

5   aglycosylated) of YebF proteins secreted from individual bacterial colonies (**Fig. 2a**).

6   Here, we hypothesized that genetic fusion of glycosite-modified POIs to YebF would

7   result in extracellular secretion of the fusion protein such that glycans installed on the POI

8   could be detected by the nitrocellulose membrane-based screening strategy. To test this

9   hypothesis, we initially focused on *E. coli* Im7 as the POI for several reasons: (i) it is a

10   small, globular 87-residue protein that lacks disulfide bonds and is well expressed in the

11   periplasm where bacterial *N*-glycosylation occurs (23); (ii) although not a native

12   glycoprotein, Im7 modified at its C-terminus with a DQNAT glycosylation tag can be

13   glycosylated by the *C. jejuni N*-glycosylation machinery in *E. coli* (23); (iii) crystal

14   structures are available for wild-type (wt) Im7 (24) and for Im7 in complex with its cognate

15   toxin colicin E7 (ColE7) (25); and (iv) a limited set of seven Im7 variants was previously

16   generated to determine the effects of $GlcNAc_2$ attachment on folding and stability (20),

17   providing some useful reference points for comparison.

18   To determine whether Im7 was compatible with the glycoSNAP procedure, *E. coli*

19   strain CLM24 was transformed with a plasmid encoding YebF-Im7 that was modified with

20   a DQNAT glycosylation tag (26) at the C-terminus of Im7 along with two additional

21   plasmids, one encoding glycosyltransferase (GT) enzymes for the biosynthesis of the *N*-

22   glycan and the other encoding the oligosaccharyltransferase (OST) for transfer of the

23   resulting *N*-glycan to acceptor proteins. To minimize microheterogeneity so that modified

24   acceptor proteins all carried identical glycans, we created a system for producing

25   homogeneous *N*-glycans with the structure $GalNAc_5(Glc)GlcNAc$, which is one of several

26   structurally related glycan donors that can be efficiently transferred to target proteins in

27   *E. coli* by the *C. jejuni* OST PglB (*Cj*PglB) (27, 28). While the biotechnological value of

28   this glycan is questionable, it served as an excellent model for our proof-of-concept

29   SSGM studies for several reasons. First, it involves formation of the key GlcNAc-Asn

30   linkage, which is the same as found in prototypic eukaryotic *N*-glycans. Second, it has the

31   potential to be remodeled as a complex-type eukaryotic glycan via a two-step enzymatic
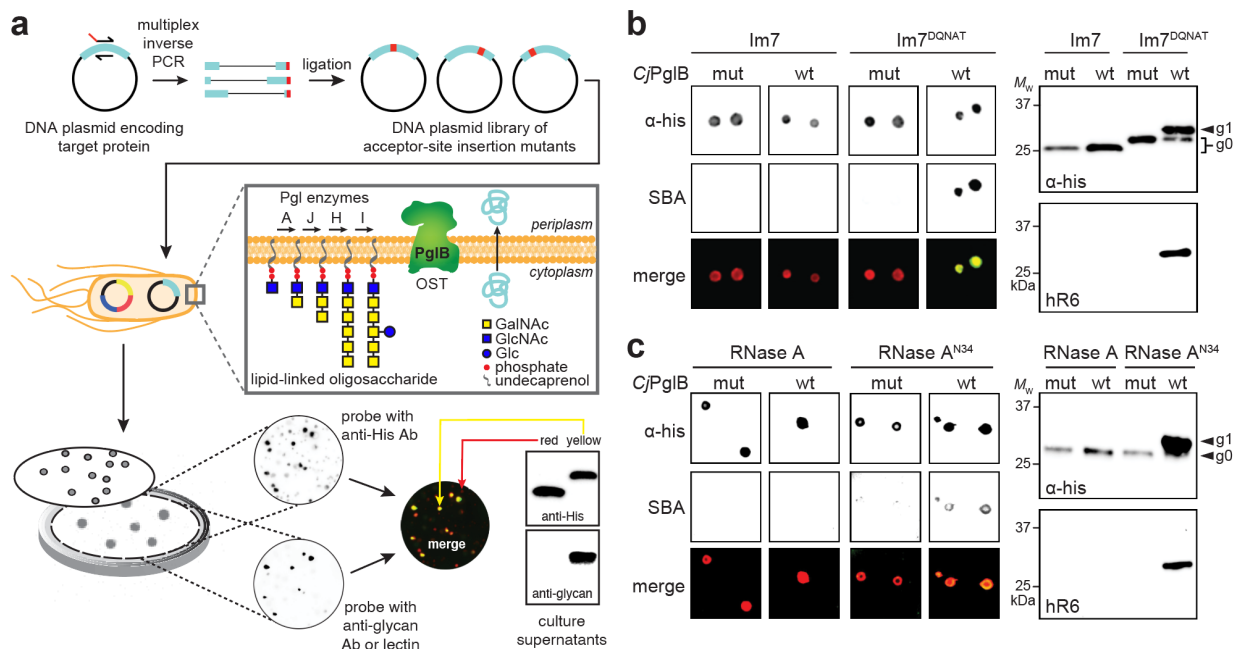
Figure 2. Construction and interrogation of SSGM libraries. (a) Schematic of SSGM library construction using multiplex inverse PCR. The resulting DNA plasmid library, encoding neoglycoprotein variants with glycosite substitutions at every possible position, was used to co-transform *E. coli* strain CLM24 along with two additional plasmids encoding the requisite *N*-glycosylation machinery from *C. jejuni*. The resulting bacterial library was plated on solid agar, after which colonies and their secreted glycoproteins were replica plated on nitrocellulose membranes as described in the text. (b) Immunoblot analysis of acceptor proteins in colony secretions (left) and extracellular supernatant fractions (right) derived from *E. coli* CLM24 carrying a plasmid encoding either YebF-Im7 or YebF-Im7^{DQNAT} along with plasmids encoding *N*-glycosylation machinery with either wild-type *Cj*PglB (wt) or an inactive mutant (mut). (c) Same as in (b) but with YebF-RNase A and YebF-RNase A^{N34} in colony secretions (left) and periplasmic fractions (right). Blots were probed with anti-polyhistidine antibody (α-His) to detect acceptor proteins and SBA or hR6 serum to detect glycans. Bottom color panels in (b) and (c) depict overlay of α-His and SBA blots (merge). Arrows denote aglycosylated (g0) and singly glycosylated (g1) forms of YebF-Im7^{DQNAT} or YebF-RNase A^{N34}. Molecular weight (M_W) markers are indicated at left. Results are representative of at least three biological replicates.

trimming/transglycosylation process (29). Third, its structural uniformity and relative abundance when produced heterologously in *E. coli* cells, as well as its compatibility with PglB, all help to ensure that differences in glycosylation efficiency are minimally affected by substrate-related factors and are instead attributable to accessibility of a given acceptor site.

When plated on solid agar and subjected to the colony-blotting method, cells expressing YebF-Im7^{DQNAT}, or a control YebF-Im7 construct that lacked the glycosylation tag, were able to secrete the fusion into the extracellular medium as evidenced by cross-reaction of an anti-His antibody with the membranes (**Fig. 2b**). However, only the strain expressing YebF-Im7^{DQNAT} in the presence of wt *Cj*PglB, but not a *Cj*PglB variant

7

1   rendered inactive by two active-site mutations (D54N and E316Q) (21), gave rise to

2   colonies that reacted with soybean agglutinin (SBA) (**Fig. 2b**), a lectin that binds terminal

3   GalNAc residues in the *C. jejuni N*-glycan (27). The colony blotting results were

4   corroborated by immunoblot analysis of culture supernatants, which revealed that YebF-

5   Im7 and YebF-Im7^{DQNAT} were both secreted into the extracellular medium but only the

6   latter was glycosylated as evidenced by the appearance of a higher molecular weight

7   band in the blot probed with glycan-specific antiserum (**Fig. 2b**). As expected, no glycan-

8   specific signal was detected in colony blots or immunoblots corresponding to cells

9   carrying the mutant *Cj*PglB enzyme (**Fig. 2b**). Importantly, the predominant glycan

10   attached to YebF-Im7^{DQNAT} corresponded to GalNAc$_5$(Glc)GlcNAc, which represented

11   >98% of all detected glycoforms as confirmed by mass spectrometry (**Supplementary**

12   **Fig. 1**). Collectively, these results confirmed the compatibility of bacterial Im7 with our

13   glycosylation workflow, yielding homogenously modified acceptor proteins that were

14   readily detected by glycoSNAP screening.

15   **Rapid identification of acceptor site permissiveness using SSGM.** Next, the plasmid

16   encoding YebF-Im7 was mutagenized to create a library of Im7 gene sequences, each

17   carrying an individual sequon substitution and cumulatively covering all positions in the

18   Im7 protein. Mutagenesis was performed using multiplex inverse PCR (30) with a set of

19   divergent abutting primers that were designed to amplify the entire plasmid and introduce

20   an acceptor asparagine residue at every position in the Im7 gene (with the two upstream

21   and two downstream residues being changed to DQ and AT, respectively), thereby

22   yielding a highly focused plasmid library enriched with in-frame clones each bearing a

23   single DQNAT acceptor motif at a defined position (**Fig. 2a**). Indeed, next-generation

24   sequencing of the pre-selected plasmid library confirmed complete sequence coverage

25   for all glycosite positions in Im7, with >10^3 reads detected for all but one position.

26   (**Supplementary Fig. 2**). With all glycosite variants present and accounted for, the

27   resulting plasmid library was introduced into strain CLM24 carrying the requisite *N*-

28   glycosylation machinery and the library-transformed cells were plated on solid agar and

29   subjected to glycoSNAP screening. From one membrane, we detected a total of ~200

30   glycosylation-positive colonies, of which 20 were randomly chosen for further analysis.

31   Sequencing confirmed that a single in-frame DQNAT motif was present in each isolated
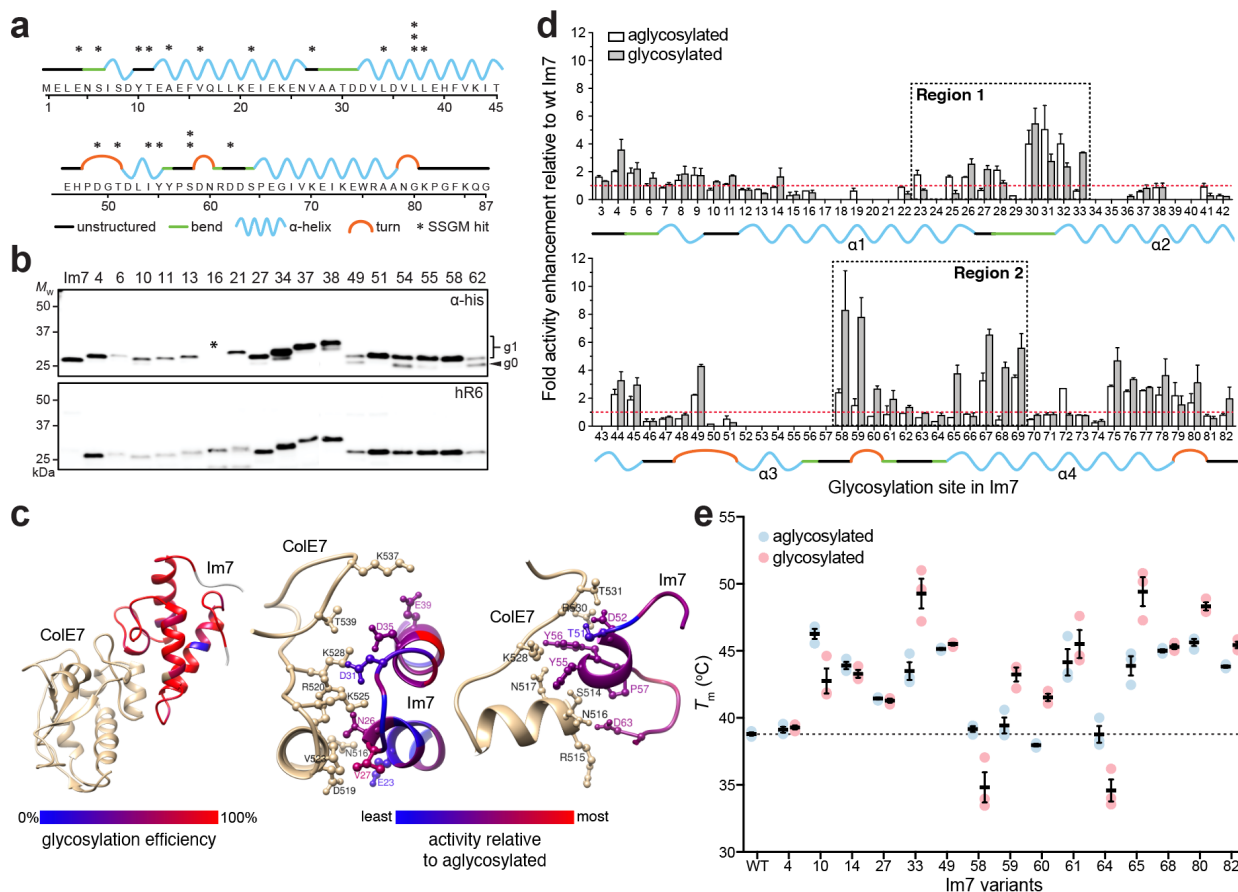
Figure 3. Construction and characterization of bacterial Im7 neoglycoprotein library. (a) Primary sequence and predicted secondary structure for *E. coli* Im7 immunity protein. Asterisks denote location and frequency of glycosite hits isolated using SSGM. Predicted structures adapted from PDB ID 1AYI. (b) Immunoblot analysis of supernatant fractions from CLM24 cells carrying plasmids encoding YebF-Im7 fusions with sequon mutations at indicated position and requisite *N*-glycosylation machinery. Blots were probed with anti-polyhistidine antibody (α-His) to detect acceptor protein (top panel) and hR6 serum against the glycan (bottom panel). Markers for aglycosylated (g0) and singly glycosylated (g1) forms of acceptor proteins are indicated at right. Molecular weight (M_W) markers are indicated at left. Asterisk indicates construct with mutation that introduced stop codon just before 6xHis tag, preventing α-His detection. Results are representative of at least three biological replicates. (c) Mapping of cell-based glycosylation efficiency onto three-dimensional structure of Im7 in complex with ColE7 (left). Heatmap analysis of the glycosylation efficiency was determined based on densitometric quantification of the percent glycosylated (defined as g1/[g0+g1] ratio) for each acceptor protein in the anti-His immunoblot. Detailed interactions between ColE7 and Im7, highlighting sidechains of Im7 in the regions of α1-loop12-α2 (residues 19-39; middle) and loop23-α3-loop34 (residues 46-63; right). Heatmap analysis of change in binding activity was determined by normalizing activity measured for glycosylated sequon variant by aglycosylated counterpart. (d) Binding activity of glycosylated (gray bars) and aglycosylated (white bars) YebF-Im7 variants recovered from supernatants was measured by ELISA with ColE7 as immobilized antigen. All data were normalized to binding activity measured for aglycosylated YebF-Im7 lacking a sequon (wt), such that values greater than 1 (denoted by dashed red line) indicate enhanced binding activity relative to wt Im7. Dashed boxes correspond to two regions (Region 1: residues 23-33; Region 2: residues 58-69) that have many variants with increased activity. Data are average of three biological replicates and error bars represent standard deviation of the mean. (e) DSF analysis of 15 most active YebF-Im7 variants with and without glycosylation. T_m calculated as midpoint of thermal transition between native and unfolded states. Dashed line indicates T_m for wt YebF-Im7 (38.6 ± 1.0 °C). Black bars are average of three independent replicates with error bars reported as standard error of the mean.

9

1   hit, with the Im7^{N37} and Im7^{N58} variants (where the superscript denotes the location of the

2   asparagine residue) occurring three and two times, respectively (**Fig. 3a**). The hits were

3   fairly evenly distributed throughout the entire Im7 sequence and situated in every type of

4   secondary structure including bends, turns, and α-helices, consistent with X-ray

5   crystallographic data showing that occupied glycosylation sites can occur on all

6   secondary structural elements (31). Immunoblot analysis confirmed that each of the

7   selected clones was efficiently glycosylated (**Fig. 3b**).

8   To exhaustively explore glycosylation sequence space, we constructed all possible

9   individual Im7 sequon variants (80 in total) using the multiplex PCR primer pairs to

10   introduce DQNAT sequons at every position of the protein. A strikingly large number (78

11   out of 80) of these variants were found to be glycosylated, many with an efficiency that

12   was at or near 100% as estimated from densitometry of the anti-His blot (**Fig. 3c** and

13   **Supplementary Fig. 3**). Because glycosylation by *Cj*PglB can occur both before and after

14   protein folding is completed (**Supplementary Fig. 4**) (32, 33), the secondary and tertiary

15   structure around a glycosylation site is likely to have a direct effect on the extent to which

16   a given site is occupied. Indeed, it has been observed that sequons located in structurally

17   defined regions of folded acceptor proteins are poorly glycosylated and that partial

18   unfolding is required to increase glycosylation efficiency at these sites (33, 34). To

19   determine if the structural context for any of the Im7 sequon variants was a determinant

20   for the timing and efficiency of glycosylation, we performed *in vitro*, cell-free glycosylation

21   reactions in which already folded but yet-to-be glycosylated YebF-Im7 proteins derived

22   from culture supernatants were incubated with purified *Cj*PglB and glycan donor.

23   Remarkably, there was near perfect agreement between the cell-free and cell-based

24   glycosylation results, with nearly all of the purified Im7 variants undergoing highly efficient

25   glycosylation that was at or near 100% with few exceptions (**Supplementary Fig. 3**). The

26   observation that so many Im7 variants were efficiently glycosylated *in vitro* by the *Cj*PglB

27   enzyme (*i.e.*, after folding had been completed) indicates that each sequon was located

28   in either a structurally compliant position (*e.g.*, flexible and surface-exposed loops) within

29   the folded protein or in a region of the protein that became partially unfolded during the

30   cell-free glycosylation reaction. While broad accessibility is certainly plausible given the

31   small size and simple topology of Im7, we cannot rule out the contribution of

1   conformational destabilizing effects caused by substitution of five-residue stretches of

2   native amino acids in the protein. Regardless of the exact reason, these results indicate

3   that Im7 was extremely tolerant to both cell-based and cell-free installation of *N*-glycans

4   over its entire structure.

5   **Structural and functional consequences of Im7 glycosylation.** To exhaustively

6   determine the effect of glycan attachment on neoglycoprotein properties, we first

7   quantified binding activity of all 80 Im7 sequon variants with and without glycosylation

8   by subjecting each to multiwell enzyme-linked immunosorbent assay (ELISA) using

9   purified ColE7 as immobilized antigen. Native Im7 interacts with ColE7, a 60-kDa

10   bacterial toxin that is cytotoxic in the absence of the cognate Im7 inhibitor (35). With an

11   eye towards multiplexibility, we chose to assay YebF-Im7 fusions directly because: (i)

12   it obviated the need for molecular reformatting of the expression constructs; (ii) the

13   fusions could be isolated as relatively pure species from cell-free supernatants,

14   bypassing the need for extensive purification; and (iii) the introduction of the small YebF

15   domain had no measurable effect on ColE7-binding activity (**Supplementary Fig. 5a**).

16   Whereas nearly two thirds of the YebF-Im7 fusions were either unaffected by

17   glycosylation or rendered inactive by introduction of the DQNAT motif alone, particularly

18   in a contiguous stretch between residues 50-57 of Im7, the remaining one third exhibited

19   significantly altered binding activity that was attributable to the presence of the *N*-glycan

20   (**Fig. 3d**). These glycosylation-induced effects were clearly dependent on the precise

21   location of the modification. Indeed, some of the most striking increases in binding activity

22   for glycosylated variants over their aglycosylated counterparts were observed to occur at

23   the transition between different types of secondary structure (*e.g.*, variants Im7^{N33}, Im7^{N58}

24   and Im7^{N65}). These results were particularly noteworthy in light of the elevated probability

25   of finding naturally occurring sequons in locations where secondary structure changes

26   (31).

27   Among the Im7 neoglycoproteins whose activity was most significantly affected

28   both positively and negatively by *N*-glycosylation, the majority were located in two distinct

29   regions covering residues 23–33 and 58–69 (**Fig. 3d**). These regions occurred within the

30   two arms of Im7 (one located in α1–loop12–α2 from residue 19 to 39 and the other in

31   loop23–α3–loop34 from residue 46 to 63) that interact extensively with a continuous

11

1   region in ColE7 in the crystal structure (**Fig. 3c**) (25). The two interfaces are charge-

2   complementary, and charge interactions are largely responsible for the tight and specific

3   binding between the two proteins; hence, it was not surprising that binding activity was

4   sensitive to *N*-glycan attachment in the vicinity of these interfaces. It should be pointed

5   out that the presence of an *N*-glycan in some of these positions was uniquely modulatory,

6   as substitution of DQNAT alone in these same locations generally had little effect on

7   activity, as evidenced by the comparable ColE7 binding measured for aglycosylated Im7

8   variants versus wt Im7 (**Supplementary Fig. 5b**).

9   To determine whether any of the glycosylation-induced increases in binding activity

10   were related to stabilization of the native fold, the most active Im7 neoglycoproteins were

11   subjected to differential scanning fluorimetry (DSF) with SYPRO Orange dye in a real-

12   time PCR instrument. Previous studies showed that melting temperature (T_m) values

13   obtained by DSF correlated well with those determined by circular dichroism (CD) thermal

14   denaturation (36). Here too, we observed excellent agreement between these two

15   methods, which both yielded T_m values for wt Im7 (~39 °C, **Supplementary Fig. 5c and**

16   **d**) that agreed with a previously reported value (35). Importantly, the presence of the small

17   YebF domain did not significantly alter the T_m value for Im7 (**Supplementary Fig. 5d**),

18   consistent with its lack of effect on ColE7-binding activity. We also confirmed that DSF

19   results obtained using YebF-Im7 derived directly from cell-free supernatants were

20   indistinguishable from those obtained with more extensively purified YebF-Im7

21   (**Supplementary Fig. 5d**). Using DSF, the average T_m values for glycosylated and

22   aglycosylated versions of each Im7 variant were measured, and the change in unfolding

23   temperature, ΔT_m, was calculated such that a positive ΔT_m signified an increase in

24   structural order and a reduced conformational flexibility due to appending a glycan.

25   Several of the variants exhibited positive ΔT_m values, with the largest increases

26   corresponding to glycan installation at N33, N59, N60, N65 and N80 (**Fig. 3e**).

27   Conversely, glycans at N10, N58, and N64 caused the largest decreases in T_m, indicative

28   of glycan-induced protein structural changes that destabilized the protein.

29   **SSGM of an acceptor protein with more complex topology.** We next turned our

30   attention to bovine RNase A. Like Im7, RNase A has been intensely studied from a

31   structure–function standpoint and has been pivotal to understanding many aspects of

1   enzymology, biological chemistry, and protein folding and stability. We chose RNase A

2   because (i) it is a relatively small, basic protein, containing 124 residues but with a more

3   complex topology than Im7, with all major types of secondary structure, namely α-helices,

4   β-sheets, and turns, represented; (ii) the natively glycosylated form of RNase A, namely

5   RNase B, contains a single *N*-linked oligosaccharide at N34 and a crystal structure is

6   available (37); (iii) glycosylation at N34 has no apparent effect on the secondary or tertiary

7   structure (37) but does appear to alter the thermal stability (38) although this is

8   controversial (39); and (iv) RNase A modified with an optimal bacterial sequon at the

9   native N34 glycosylation site (RNase A^{N34}) can be glycosylated by *Cj*PglB in both cell-

10   based and cell-free reactions (32, 33). For these reasons, RNase A represented an ideal

11   target for SSGM.

12   Extracellular secretion of glycosylated YebF-RNase A^{N34} was observed in colony

13   blots and immunoblots (**Fig. 2c**), confirming the compatibility of RNase A with glycoSNAP

14   screening. An SSGM library was created by subjecting YebF-RNase A plasmid DNA to

15   the multiplex inverse PCR method, resulting in sequence coverage of 93% in the pre-

16   selected library as determined by next-generation sequencing (**Supplementary Fig. 2**).

17   CLM24 cells carrying plasmids encoding the requisite *C. jejuni* glycosylation machinery

18   were transformed with the SSGM library and subjected to glycoSNAP screening. A total

19   of ~100 glycosylation-positive colonies were randomly selected from two membranes and

20   subjected to sequencing analysis. Of these, only 50 were non-redundant as many of the

21   sequences were isolated multiple times (*e.g.*, seven times each for RNase A^{N41} and

22   RNase A^{N122}; **Fig. 4a**). The sequons of these positive hits were uniformly distributed

23   throughout the primary sequence and found in every type of secondary structural

24   element, akin to the results with Im7. Immunoblot analysis confirmed that all selected

25   clones were glycosylated, and the efficiency for most was at or near 100% as estimated

26   by densitometry analysis of the anti-His blots (**Fig. 4b** and **Supplementary Fig. 6a and**

27   **b**). We also performed theoretical analysis of each of these RNase A glycosite variants

28   in   terms   of   glycosylation   probability   using   NetNGlyc1.0

29   (http://www.cbs.dtu.dk/services/NetNGlyc/), a web-based tool that predicts *N*-

30   glycosylation sites in human proteins using artificial neural networks that examine the

31   sequence context of N-X-S/T sequons (40). Interestingly, a total of 18 glycosites, which

13
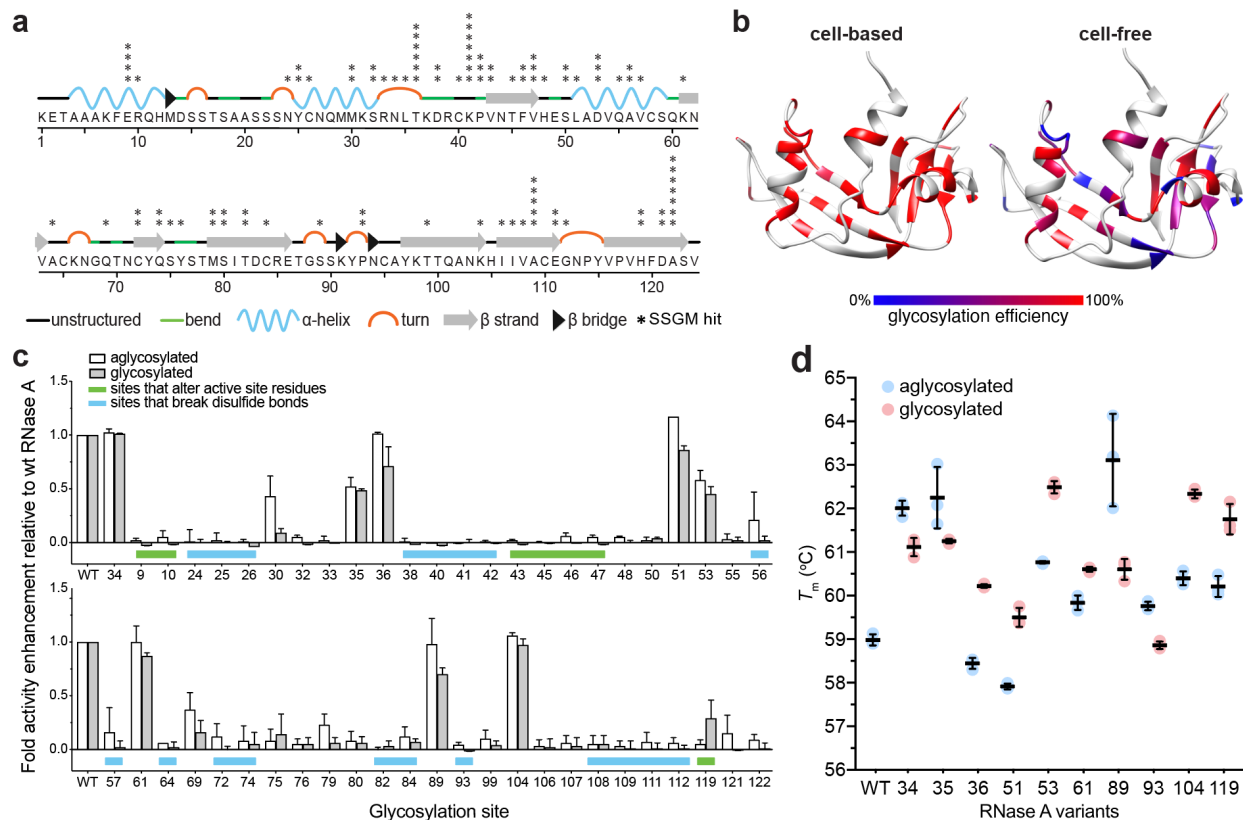
Figure 4. Construction and characterization of RNase A neoglycoprotein libraries. (a) Primary sequence and predicted secondary structure for bovine pancreatic RNase A. Asterisks denote location and frequency of glycosite hits isolated using SSGM. Predicted structures adapted from PDB ID 1RBX. (b) Mapping of cell-based (left) and cell-free (right) glycosylation efficiency onto three-dimensional structure of RNase A. Heatmap analysis of glycosylation efficiency was determined based on densitometric quantification of percent glycosylated (defined as g1/[g0+g1] ratio) for each neoglycoprotein in anti-His immunoblot. (c) Enzymatic activity of glycosylated (gray bars) and aglycosylated (white bars) RNase A variants recovered from culture supernatants. All data were normalized to binding activity measured for aglycosylated YebF-RNase A lacking a sequon (wt). Data are average of three biological replicates and error bars represent standard deviation of the mean. (d) DSF analysis of YebF-RNase A variants with and without glycosylation. T_m was calculated as midpoint of thermal transition between native and unfolded states. Dashed line indicates T_m for wt YebF-RNase A (59.0 ± 0.1 °C). Black bars are average of three independent replicates with error bars reported as standard error of the mean.

were predominantly clustered in the C-terminal half of the protein, had a glycosylation probability score below 50% (**Supplementary Fig. 6c**) and thus would be predicted to inefficiently glycosylated, if at all. RNase A^{N111} and RNase A^{N122}, in particular, both scored below 30% and yet were both very efficiently glycosylated in cells (and *in vitro*, as discussed below).

To investigate whether the structural context of the sequon impacted the possible timing of PglB-mediated glycan installation, we performed *in vitro*, cell-free glycosylation

1   of folded RNase A variants. While some variants were glycosylated equally well in cell-

2   based and cell-free reactions (*e.g.*, RNase A^{N46} and RNase A^{N64}), an unexpectedly large

3   number showed significantly lower levels of glycosylation under cell-free conditions (**Fig.**

4   **4b** and **Supplementary Fig. 6a and b**). Most notably among these were variants N34,

5   N35, N36, N43, N51, N61, N69, N72, N80, N89, and N104, which were all efficiently

6   glycosylated in cells but underwent little or no detectable glycosylation *in vitro*. These

7   sequons occur at locations that were likely to be accessible to the OST during

8   translation/translocation when the proteins are unfolded but became inaccessible after

9   the protein completed folding. Indeed, the native *N*-glycosylation site at N34 is located in

10   a structured domain, suggesting that the poor cell-free glycosylation at this specific

11   location (and perhaps also at the nearby N36 and N43 sites) was due to sequon

12   inaccessibility in the folded state. Such folding-dependent recognition of this site has been

13   observed previously (32, 33) and, together with the results presented here, supports a

14   model whereby cell-based glycosylation of these particular sequons involves glycan

15   installation prior to folding, either co- or post-translocationally (**Supplementary Fig. 4**).

16   To determine the consequences of glycosylation at the 50 unique sites, the ability

17   of glycosylated and aglycosylated versions of each sequon variant to catalyze the

18   hydrolysis of the phosphodiester bonds in RNA was evaluated. While the addition of YebF

19   had little to no effect on RNase A activity (**Supplementary Fig. 7a**), more than half of the

20   RNase A variants were inactivated by substitution of the DQNAT sequon (**Fig. 4c**). To

21   determine if this might be due to the substitution of five residues in the target protein, a

22   requirement for optimal recognition by *Cj*PglB (41), we mutated RNase A more

23   conservatively at a select number of sites. Specifically, we generated minimal sequons

24   (D-X-N-X-T/S or X-X-N-X-T/S, where X represents the native amino acid), which in most

25   cases required only 1 or 2 amino acid changes. Each of these mutants was completely

26   inactive except for RNase A^{N55} with a DVNAT sequon, which retained some activity but

27   was still significantly less active than the wt enzyme (**Supplementary Fig. 7b**). Hence,

28   even relatively minor sequence perturbations at these positions, in addition to the less

29   subtle substitution with DQNAT, were all capable of inactivating RNase A. More careful

30   inspection revealed that the majority of variants with little to no activity corresponded to

1   the substitution of sequons in locations that would be predicted to disrupt catalytically

2   important residues or disulfide bonds (**Fig. 4c** and **Supplementary Results**).

3   Among the RNase A neoglycoproteins that retained function, only eight (sequons

4   at N34, N35, N36, N51, N53, N61, N89, and N104) showed activity that was on par

5   (>50%) with wt RNase A but none were more active than their aglycosylated counterpart

6   (**Fig. 4c**). In the case of RNase A^{N119}, introduction of the DQNAT sequence completely

7   abrogated catalytic activity, consistent with previous findings that the relative activity of

8   an H119N mutant was reduced to less than 1% of wt RNase A, with k_{cat}/K_M values reduced

9   by 100- to 1000-fold depending on the substrate used (42). Despite the importance of this

10   residue for catalysis, glycosylation at this position partially restored enzymatic activity,

11   indicating an *N*-glycan-dependent gain-of-function.

12   To determine whether glycosylation impacted stability, we again used DSF to

13   analyze the most active RNase A neoglycoproteins along with RNase A^{N93}, which was

14   randomly chosen as a representative inactive variant. The measured T_m values for wt

15   YebF-RNase A and its unfused counterpart were both ~59 $^{\circ}$C (**Supplementary Fig. 7c**),

16   in close agreement with previous findings (39), while the T_m values for all the YebF-RNase

17   A variants spanned a range from 58–63 $^{\circ}$C (**Fig. 4d**). Most exhibited positive ΔT_m values

18   compared to their aglycosylated counterpart, including the RNase A^{N119} variant,

19   suggesting that the restoration of activity caused by glycan attachment at N119 also

20   served to stabilize the protein. In contrast, RNase A^{N89} and RNase A^{N93} exhibited large

21   negative ΔT_m values that coincided with slightly weakened activity due to glycan

22   attachment in the case of N89 and complete inactivation in the case of N93.

23   **Investigation of IgG variable domain glycosylation using SSGM.** We next

24   investigated antibody variable domain glycosylation, a phenomenon that is observed for

25   ~15% of serum IgGs and contributes to diversification of the B-cell antibody repertoire

26   (6). Although glycan installation within the variable domains of Fab arms has been long

27   known, the rules governing the selection of *N*-glycosylation sites in Fab domains that

28   emerge during somatic hypermutation and the functional consequences of the attached

29   glycans remain poorly understood. To systematically investigate this phenomenon using

30   SSGM, the two variable domains, V_H and V_L, from the human anti-HER2 monoclonal

31   antibody were joined by a flexible linker to form scFv-HER2 that was subsequently

1   modified at its N-terminus with YebF and at its C-terminus with a DQNAT motif.

2   Extracellular secretion of glycosylated YebF-scFv-HER2^{DQNAT} was observed in colony

3   blots and immunoblots (**Fig. 5a**), confirming the compatibility of scFv-HER2 with

4   glycoSNAP screening. Because variable domain glycosylation is subject to selection

5   mechanisms that depend on the nature of the antigen (6), we modified the SSGM strategy

6   to enable dual screening of glycosylation and antigen-binding activity by labeling colonies

7   with SBA lectin and the extracellular domain (residues 1-652) of human HER2 (HER2-

8   ED), which was avidly bound by scFv-HER2^{DQNAT} fused to YebF (**Supplementary Fig.**

9   **8a**). In this way, two-color screening could be used to identify colonies that were positive

10   both for glycosylation and for antigen binding, as demonstrated with the YebF-scFv-

11   HER2^{DQNAT} construct (**Fig. 5a**). Next, we constructed and screened an SSGM library,

12   after which two-color glycoSNAP screening was performed with CLM24 cells carrying

13   plasmids encoding the library and the *C. jejuni* glycosylation machinery. A total of ~60

14   dual-positive hits were isolated from membranes, of which 21 were determined to be non-

15   redundant (*e.g.*, N58 in V_L and N42 in V_H were each isolated 12 times) (**Fig. 5b**) and

16   subsequently confirmed for extent of glycosylation by immunoblot and densitometry

17   analysis (**Supplementary Fig. 8b and c**). The sequons of these hits were sparsely

18   distributed throughout the primary sequence, with a large proportion clustering just after

19   the second and third complementarity-determining regions (CDRs) of the V_L domain and

20   also in the flexible linker, indicating a clear selection bias for specific sites that tolerated

21   glycosylation without interfering with binding function. Interestingly, a few of the identified

22   sequons occurred in CDR2 of the V_L domain and CDR1 and CDR2 of the V_H domain,

23   consistent with naturally occurring IgG repertoires in which *N*-glycosites are found

24   preferentially in the CDRs (6).

25   In terms of function, all 21 scFv-HER2 hits exhibited HER2-ED binding activity

26   above background (**Fig. 5c**), which was expected given that the screening process was

27   adapted to include antigen binding. Importantly, nine of these neoglycoproteins (N58,

28   N64, and N109 in V_L; N3, N4, N9, N10 in linker; N42 and N113 in V_H) exhibited increased

29   binding compared to their aglycosylated counterpart, and most of these were also more

30   active than the parental scFv-HER2. For the five clones exhibiting the greatest increase

31   in activity due to glycosylation, we measured T_m values and found that in general glycan
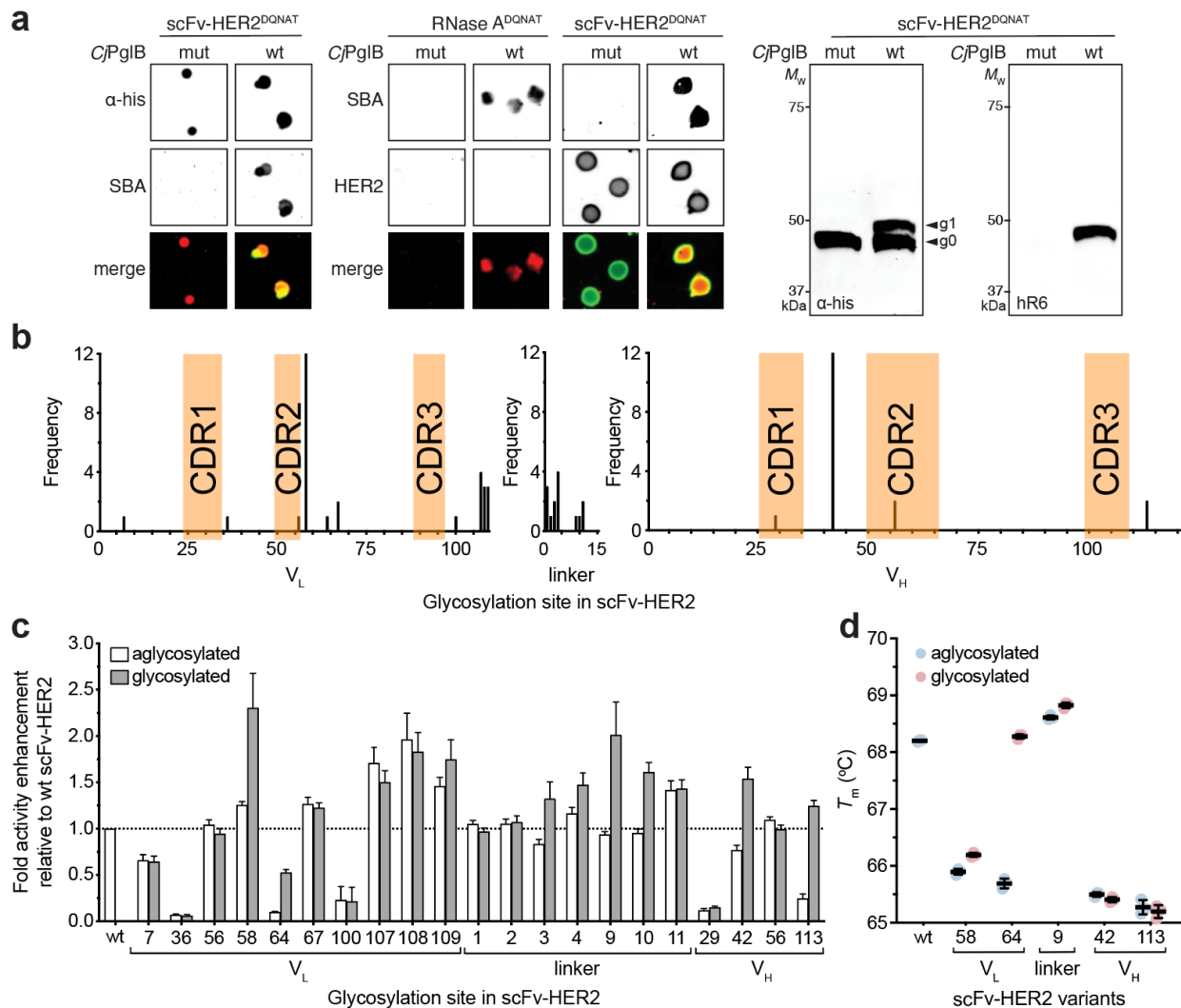
17

1
2
3 **Figure 5. Construction and characterization of scFv-HER2 neoglycoprotein libraries.** (a) Immunoblot
4 analysis of acceptor proteins in colony secretions (left and middle) and periplasmic fractions (right) derived
5 from *E. coli* CLM24 carrying plasmids encoding scFv-HER2^{DQNAT} and requisite N-glycosylation machinery
6 with either wild-type *Cj*PglB (wt) or an inactive mutant (mut). Blots were probed with anti-polyhistidine
7 antibody (α-His) to detect acceptor protein, SBA or hR6 serum to detect the glycan, and HER2-ED to detect
8 antibody binding. Bottom color panels depict overlay of α-His and SBA blots or SBA and HER2 blots
9 (merge). Arrows denote aglycosylated (g0) and singly glycosylated (g1) forms of scFv-HER2^{DQNAT}.
10 Molecular weight (M_W) markers are indicated at left. Results are representative of at least three biological
11 replicates. (b) Frequency and position of N-glycosylation sites in scFv-HER2^{DQNAT} glycovariants isolated
12 using SSGM. (c) Binding activity of glycosylated (gray bars) and aglycosylated (white bars) scFv-
13 HER2^{DQNAT} variants as measured by ELISA with HER2-ED as immobilized antigen. All data were
14 normalized to binding activity measured for aglycosylated scFv-HER2 lacking a sequon (wt), such that
15 values greater than 1 (denoted by dashed line) indicate enhanced binding activity relative to wt scFv-HER2.
16 Data are average of three biological replicates and error bars represent standard deviation of the mean. (d)
17 DSF analysis of YebF-scFv-HER2 variants with and without glycosylation. T_m was calculated as midpoint
18 of thermal transition between native and unfolded states. Dashed line indicates T_m for wt YebF-scFv-HER2
19 (68.2 ± 0.1 °C). Black bars are average of three independent replicates with error bars reported as standard
20 error of the mean.
21
22

18

1 attachment did not affect stability (**Fig. 5d**). However, the one exception was N64 V_L,

2 which experienced a 2.6 °C increase in T_m due to the addition of the *N*-glycan. Overall,

3 these results are in agreement with several previous studies showing that variable region

4 glycans contribute to antibody binding characteristics and stability in a manner that

5 depends on the precise location of the glycan (6, 43) and suggest that glycosylation in

6 this region may be a useful strategy for fine-tuning the performance of IgG antibodies and

7 their engineered derivatives.

8 **Computational analysis of neoglycoproteins.** To test whether protein-structure

9 analyses could explain the observed effects of sequon substitution and glycosylation, we

10 modeled the sequon-substituted variants, with and without glycosylation, and calculated

11 simple geometric measures (secondary structure, burial, distance to the binding site, and

12 surface area) as well as Rosetta energy estimates (stability and interface score) for each.

13 Unfortunately, none of these factors were found to correlate significantly with the activity

14 or stability of the Im7 or RNase A neoglycoproteins (**Supplementary Figs. 9-13**; and

15 **Supplementary Results**). It should be noted that these metrics may be less useful for

16 RNase A because the activities are primarily explained by the disruption of the active site

17 and the disulfide bonds, which are not captured in these metrics. We also generated

18 ensembles of glycan conformations for several Im7 neoglycoproteins, including several

19 with increased (Im7^{N30}, Im7^{N49}, and Im7^{N58}) and one with decreased (Im7^{N31}) activity due

20 to glycosylation, in the context of binding to E7. These ensembles revealed that: (i) the

21 glycan and the bound protein often interact to change the binding activity positively or

22 negatively; and (ii) enhanced binding appears to be mediated by multiple low-energy

23 glycan conformations making favorable interactions with E7 (**Supplementary Fig. 14**;

24 and **Supplementary Results**).

25 Next, we compared the experimental binding activity for scFv-HER2 with multiple

26 geometric and Rosetta metrics. Unlike Im7 or RNase A, scFv-HER2 activity correlated

27 with many of our metrics. First, sequon burial reduces the binding affinity of scFv-HER2

28 for its antigen both in the glycosylated ($R^2 = 0.43$) and aglycosylated ($R^2 = 0.21$) states

29 (**Fig. 6a** and **Supplementary Fig. 9b**, respectively). Similarly, the closer the sequon was

30 to the paratope, the greater the likelihood of reduced activity for the glycosylated ($R^2 = $

31 0.23) and aglycosylated ($R^2 = 0.20$) variants (**Fig. 6b** and **Supplementary Fig. 9c**,

19
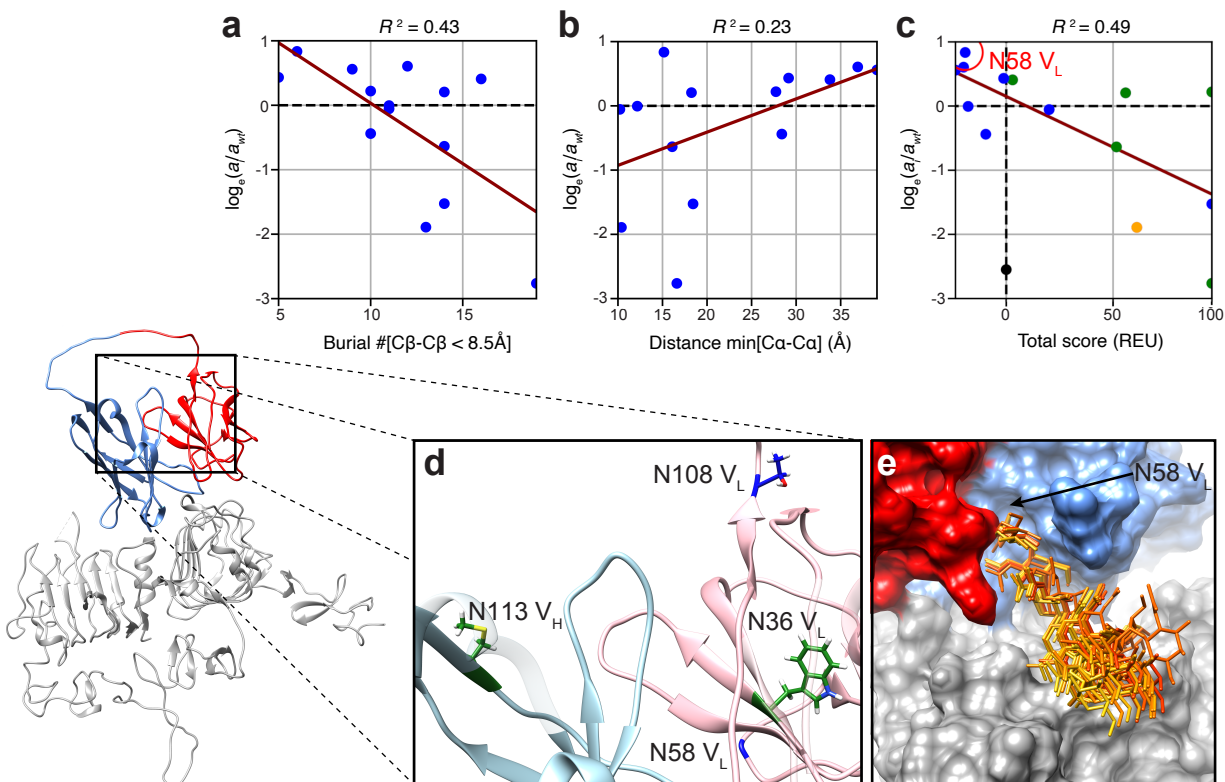
1

2 **Figure 6: Computational analysis of scFv-HER2 neoglycovariants.** The structure of scFv-HER2 V_L
3 (red) and V_H (blue) domains in complex with HER2 protein (gray) is shown at bottom left. Regression
4 analyses of log activity ratio (glycosylated / wild-type) versus (a) burial of sequon substitution site, (b)
5 distance of closest HER2 residue from the sequon substitution site, and (c) total Rosetta score. In all three
6 panels, the dark red lines are the respective regression lines. Colors of dots in (c) show the respective
7 secondary structure of the sequon substitution site. Orange, green, and blue correspond to α-helix, β-
8 strand, and loop regions, respectively. N58 V_L (red circle) has the highest glycosylated binding activity
9 increase and is discussed in the text. (d) Wild-type representation of sites used for analysis of sequon
10 substitution (36 V_L, 108 V_L, and 113 V_H) and glycosylation (58 V_L). Side-chain colors reflect their respective
11 secondary structures. (e) Glycan arrangement (orange sticks) from eight low energy conformations of
12 glycosylated N58 V_L variant of scFv-HER2, revealing possible glycan-HER2 interaction responsible for
13 binding activity improvement.

14

15 respectively). The buried surface area also correlated with the activity of the glycosylated

16 variant (R^2 = 0.19, **Supplementary Fig. 10e**). The strongest predictors, however, were

17 the Rosetta scores. For the glycosylated state, the activity correlated with both the total

18 Rosetta score (R^2 = 0.49, **Fig. 6c**) and the interface score (R^2 = 0.63, **Supplementary**

19 **Fig. 10g**). The aglycosylated antibody–antigen complex total score correlated with

20 experimental binding activity (R^2 = 0.49, **Supplementary Fig. 9f**). These Rosetta scores

21 were primarily driven by the van der Waals complementarity and to a lesser extent

22 electrostatics (**Supplementary Figs. 11** and **12**).

1   For the aglycosylated activities, we selected three variants for deeper analysis: two

2   variants that had low binding activity and a poor Rosetta score (N36 V_L, N113 V_H; black

3   circles in **Supplementary Fig. 11a**) and one variant with high activity and a favorable

4   Rosetta score (N108 V_L; red circle in **Supplementary Fig. 11a**). Both N36 V_L and N113

5   V_H sites are situated on β-strands in compact regions of the anti-HER2 antibody on the

6   side opposite the antigen-binding site (**Fig. 6d**, green sticks). The reduced stability arises

7   from the steric clash of substituting a sequon inside (or near) a close-packed region of

8   the protein (Rosetta terms for steric clashes (vdW_rep) of 90.2 and 79.8 Rosetta energy

9   units (REU) for the N36 V_L and N113 V_H, respectively). When glycosylated, the clashes

10   worsen in the Rosetta models, corresponding to low activity (black circles in

11   **Supplementary Fig. 11a**). On the other hand, site N108 V_L is located at the C-terminal

12   end of V_H (**Fig. 6d**, blue sticks). Sequon substitution had a relatively small effect on the

13   electrostatic interactions (−6.2 REU) and a greater effect on the repulsive van der Waals

14   terms (−28.0 REU), indicating that new side chains are acceptable in less compact

15   regions. A similar outcome was reported following substitution mutation of a human

16   monoclonal antibody (44).

17   To understand how *N*-glycosylation was able to improve binding activity, we

18   selected mutant N58 V_L because the aglycosylated variant was 26% more active than the

19   wt scFv-HER2 and glycan addition improves the binding an additional 1.8-fold. Residue

20   N58 V_L resides in the turn between strands 1 and 2 (**Fig. 6d**, blue backbone). From

21   Rosetta-generated glycosylated structures, the low-energy states showed interfacial

22   contacts between the glycan and the surface residues of HER2 (**Fig. 6e**), improving both

23   the total Rosetta score and the interface score (red circle in **Fig. 6c** and **Supplementary**

24   **Fig. 10g**) and explaining the binding activity improvement as resulting from favorable

25   glycan-antigen contacts.

26

27   **Discussion**

28   In this study, we developed a new protein engineering workflow called SSGM for

29   constructing large neoglycoprotein libraries of virtually any POI and characterizing the

30   consequences of glycan installation. The utility and flexibility of this technique was

31   demonstrated using three structurally and functionally diverse acceptor proteins: bacterial

1   Im7, bovine RNase A, and human scFv-HER2. Specifically, each of these proteins was

2   subjected to a systematic "sequon walking" procedure that enabled creation of synthetic

3   gene libraries in which *N*-glycosylation sites (the majority of which were naïve) were

4   introduced at every possible position of the POI. Upon screening these libraries using

5   glycoSNAP (21), numerous positions in each protein were found to be efficiently *N*-

6   glycosylated. While extended regions and loops tended to be more receptive to

7   glycosylation, all types of secondary structure were found to be glycosylated, consistent

8   with the observation that naturally occurring *N*-glycans also exist on all forms of

9   secondary structure (31). For RNase A, in particular, a significant number of the efficiently

10   glycosylated sites (18/50) were predicted to have very low glycosylation potential,

11   highlighting the need for large-scale experimental studies of glycosylation, such as

12   described here, that can be used to help refine predictive tools. To this end, higher

13   throughput techniques that leverage mass spectrometry for quantitatively resolving

14   glycosylation efficiency (45, 46) could enable further refinement of the method in the

15   future.

16   The studies performed here also provided insight on the possible timing and impact

17   of glycosylation with respect to the folding process. For instance, Im7 tolerated a glycan

18   at almost every position, even when the target asparagine side chain pointed inward and

19   was considered buried (*e.g.*, positions N7, N68, and N76). Because these buried

20   positions physically cannot be glycosylated by PglB when the target protein is in the folded

21   state, they must either be glycosylated co-translationally or during a fluctuation to a

22   partially unfolded state that provides access to that site. Then, after glycosylation,

23   because Im7 presumably cannot fold back into the native structure, it must adopt a

24   different conformation to accommodate the newly added glycan, which would be feasible

25   in light of the fact that Im7 is very flexible (47). In the case of RNase A, several sites were

26   identified (*e.g.*, N34, N36) that could be efficiently glycosylated in cells but underwent little

27   to no glycosylation *in vitro* (in the already folded state), providing clear evidence for glycan

28   installation prior to folding and in a manner that may resemble the co-translocational

29   process in mammalian cells (48). The overall less efficient glycosylation seen for many

30   RNase A variants was also consistent with the protein adopting a more stable folded

31   structure compared to Im7 and providing less accessibility to buried sites.

1   In addition to uncovering glycosylatable sites, the SSGM workflow also allowed

2   the effects of these site-directed glycan "mutations" to be probed for their contribution to

3   the biological and biophysical properties of each POI. In this way, SSGM is conceptually

4   analogous to combinatorial alanine-scanning mutagenesis, which allows systematic

5   determination of the importance of individual amino acids to protein structure and function

6   (49-51). Consistent with the known modulatory effects of *N*-glycans (4, 5), many of the

7   neoglycoprotein derivatives of Im7, RNase A and scFv-HER2 exhibited detectably altered

8   stability and activity that resulted from covalent attachment of *N*-glycans at precise

9   locations in the protein backbone. For example, installing *N*-glycans in the center of α-

10   helices negatively affected activity (*e.g.*, positions 19, 42, 72 in Im7) whereas those

11   installed at the transition between different types of secondary structure and at turns

12   between motifs promoted enhanced activity and, in some cases, stability (*e.g.*, positions

13   33, 49, 58, 59, 60, 61, 65, 67, 68, 69, 78, 80 in Im7). These findings generally agreed with

14   the folding and stability effects contributed by attachment of a $GlcNAc_2$ disaccharide to

15   discrete locations in Im7 (20) and also provide clues for why natural *N*-glycosylation sites

16   occur with elevated frequency in turns and bends and especially at points of change in

17   secondary structure and with low frequency within ordered helices (31). Despite the

18   overall agreement with previous studies, a few notable differences emerged. For

19   example, in our hands, Im7 glycosylated at position 27 with the $GalNAc_5$(Glc)GlcNAc

20   heptasaccharide was more active but equally stable as its aglycosylated counterpart,

21   whereas an EPL-derived Im7 modified with chitobiose at residue 27 was significantly

22   more stable than unmodified Im7 (note that activity data was not reported) (20). Likewise,

23   RNase A^{N34} glycosylated with $GalNAc_5$(Glc)GlcNAc exhibited activity that was nearly

24   identical to that of aglycosylated RNase A^{N34} (and wt RNase A), whereas the attachment

25   of oligomannose glycans at N34 was previously observed to reduce activity by more than

26   threefold (52). The notion that discrete glycan structures attached to the same site in a

27   protein can have disparate effects is not unprecedented, having been documented for

28   other glycoproteins (53) (54). Thus, in the future, it will of interest to extend SSGM for use

29   with alternative glycan structures, including for example $Man_3GlcNAc_2$ or other human *N*-

30   and *O*-linked glycans that have been engineered in *E. coli* (32, 55, 56), so that the

23

1   consequences of varying glycan structures at discrete locations can be systematically

2   investigated.

3   The fact that *N*-glycan attachment significantly increased the binding activity of

4   several glycosite variants of Im7 and scFv-HER2 suggests that SSGM may become a

5   useful tool for adding *N*-glycans to naïve sites in proteins for tuning their biological and

6   biophysical properties. The discovery of such sites was accelerated by the ability of

7   SSGM to furnish an unprecedentedly large number of intact neoglycoproteins (a total of

8   151 in this study alone), for which the effects of *N*-glycan installation can be readily

9   catalogued using multiplexable assays for protein structure and activity as we showed

10 here. While no definitive rules regarding the effects of glycosylation were revealed here,

11 we anticipate that sequon walking on a larger, even proteome-wide, scale could provide

12 access to datasets that might allow the effects of glycosylation to be more widely

13 generalized and perhaps even predicted. Nonetheless, computational analysis indicated

14 that interactions between the glycan and the bound protein can alter binding activity

15 (positively or negatively) and that enhanced binding likely arises from low-energy glycan

16 conformations making favorable interactions with the binding partner. For example, the

17 Im7^{N58} variant that underwent the largest increase in binding activity upon glycosylation

18 also acquired new contacts with its binding partner, E7, through the glycan, which

19 strengthened binding activity 3.5-fold. Likewise, for the scFv-HER2 mutant N58 V_L, which

20 exhibited measurably higher antigen-binding activity compared to parental scFv-HER2,

21 the heptameric glycan created new contacts between scFv-HER2 and HER2-ED and

22 buried more surface area upon binding. Thus, even though part of the enhanced binding

23 was from the sequon substitution alone, perhaps from the additional contacts of the long

24 Q57 side chain or from a stabilizing effect of the sequon on the CDR L2 loop (residues

25 51-57 in V_L), most of the effect was from the *N*-glycan itself. Importantly, this observation

26 was in line with previous findings that glycans attached near (but not within) the antigen-

27 binding site can increase affinity (57). Taken together, our findings suggest that SSGM

28 could be used to rapidly identify naïve sites along a protein backbone for strategic

29 placement of *N*-glycans that substantially enhance the biological and/or biophysical

30 properties of the resulting neoglycoprotein.

31

1 **Materials and Methods**

2 **Strains and culture conditions.** *E. coli* strain DH5α was used for all molecular biology,

3 including plasmid construction, site-directed mutagenesis, and SSGM library

4 construction. BL21(DE3) was used to purify ColE7 that was used to measure Im7

5 binding activity in ELISA format. All glycosylation studies were performed using *E. coli*

6 strain CLM24 (58), which was initially grown at 37 °C in Luria–Bertani (LB) medium

7 containing appropriate antibiotics at the following concentrations: 20 μg/mL

8 chloramphenicol (Cm), 100 μg/mL trimethoprim (Tmp), and 50 μg/mL spectinomycin

9 (Spec). When cells reached mid-log phase, protein expression was induced by adding

10 0.1 mM isopropyl-β-D-thiogalactoside (IPTG) and 0.2% (v/v) L-arabinose, after which cells

11 were grown at 30 °C for 16–20 h.

12 **Plasmid construction.** For expression of the glycosylation machinery, plasmid pMAF10

13 encoding *Cj*PglB (58) along with either plasmid pMW07-pglΔB (21) or pMW07-

14 pglΔBCDEF were used. The latter plasmid was constructed by deleting the *pglCDEF*

15 genes from plasmid pMW07-pglΔB (21), resulting in a modified *C. jejuni* glycan

16 biosynthesis pathway that excluded the *pglB* gene encoding the OST and also the

17 *pglCDEF* genes encoding enzymes for synthesis and transfer of bacillosamine as

18 described previously (27). This deletion can be complemented by *E. coli* WecA, a sugar-

19 phosphate transferase that transfers GlcNAc phosphate to undecaprenol phosphate,

20 therefore initiating LLO biosynthesis. It should be noted that while pMW07-pglΔB encodes

21 the bacillosamine-related *pglCDEF* genes, we did not detect the presence of

22 bacillosamine in any of the glycoforms produced by cells carrying this plasmid. A

23 derivative of pMAF10 that encoded a catalytically inactive version of *Cj*PglB carrying

24 two active-site mutations (D54N and E316Q) (21) was used as a negative control. The

25 plasmids pTrc99S-YebF-Im7 and pTrc99S-YebF-Im7[DQNAT] were constructed by inserting

26 cloning cassettes YebF[N24L]-XbaI-Im7-SalI-FLAG-6xHis and YebF[N24L]-XbaI-Im7-BamHI-

27 DQNAT-SalI-FLAG-6xHis, respectively, into the SacI and HindIII sites of pTrc99S (59).

28 The genes encoding RNase A and scFv-HER2 were PCR amplified from plasmids pTrc-

29 ssDsbA-RNaseA (21) and pMAZ360–cIgG–Herceptin (60), respectively, and cloned into

30 the cassette between XbaI and SalI sites in pTrc99S-YebF-Im7 or XbaI and BamHI sites

31 in pTrc99S-YebF-Im7[DQNAT], replacing Im7 and Im7[DQNAT], respectively. The pTrc-spDsbA-

25

1   POI plasmids (where POI corresponds to each of the proteins of interest, namely Im7,

2   RNase A, and scFv-HER2) were cloned by one-step PCR integration of primers encoding

3   the *E. coli* DsbA signal peptide (spDsbA) into each pTrc99S-YebF-POI plasmid as

4   templates followed by Gibson assembly. PCR products were subjected to DpnI digestion

5   to remove parental plasmid. The resulting PCR products were assembled by Gibson

6   assembly and used to transform *E. coli* cells to obtain the desired plasmids. Plasmid

7   pET28-ColE7 (H569A) was constructed by inserting DNA encoding the ColE7 H569A

8   variant (61) bearing a C-terminal 6×His tag (Integrated DNA Technologies) into the NcoI

9   and SalI sites of pET28a. All plasmids were confirmed by DNA sequencing at the

10   Biotechnology Resource Center of the Cornell Institute of Biotechnology.

11   **SSGM library construction.** SSGM mutagenesis libraries were constructed by multiplex

12   inverse PCR (30) followed by T4 ligation. Each of the pTrc99S-YebF-POI plasmids was

13   used as template for PCR amplification using primer sets specifically designed such that

14   the DNA sequence 5′-GAT CAG AAT GCG ACC-3′ was included in the 5′ end of every

15   forward primer to enable substitution of the adjacent five amino acids with DQNAT. Prior

16   to PCR, the forward primers were phosphorylated using T4 polynucleotide kinase (New

17   England Biolabs) to facilitate T4 ligation later. PCR reactions were performed using

18   Phusion polymerase (New England Biolabs), and the PCR products were gel-purified

19   from the product mixtures to eliminate non-specific PCR products. The resulting PCR

20   products were self-assembled using T4 ligase (New England Biolabs) to obtain the

21   desired SSGM plasmid libraries, which were subsequently used to transform highly

22   competent DH5α cells and then isolated using a QIAprep Spin Miniprep Kit (Qiagen)

23   according to manufacturer's instructions. For next-generation sequencing, see

24   **Supplementary Methods**.

25   **GlycoSNAP assay.** Screening of SSGM libraries was performed using glycoSNAP as

26   described previously (21). Briefly, *E. coli* strain CLM24 carrying pMW07-pglΔB and

27   pMAF10 was transformed with corresponding SSGM library plasmids, and the resulting

28   transformants were grown on 150-mm LB-agar plates containing 20 µg/mL Cm, 100

29   µg/mL Tmp, and 50 µg/mL Spec overnight at 37 °C. The second day, nitrocellulose

30   transfer membranes were cut to fit 150-mm plates and pre-wet with sterile phosphate-

31   buffered saline (PBS) before placement onto LB-agar plates containing 20 µg/mL Cm,

1   100 µg/mL Tmp, 50 µg/mL Spec, 0.1 mM IPTG, and 0.2% (w/v) L-arabinose. Library

2   transformants were replicated onto 142-mm nitrocellulose membrane filters (Whatman,

3   0.45 µm), which were then placed colony-side-up on transfer membranes and incubated

4   at 30 °C for 16 h. The nitrocellulose transfer membranes were washed in Tris-buffered

5   saline (TBS) for 10 min, blocked in 5% bovine serum albumin for 30 min and probed for

6   1 h with fluorescein-labeled SBA (Vector Laboratories, catalog # FL-1011) and Alexa

7   Fluor 647® (AF647)-conjugated anti-His antibody (R&D Systems, catalog # IC0501R) or

8   HER2-ED (R&D Systems, catalog # 10126-ER) that was conjugated with Alexa Fluor

9   647^{TM} (AF647) (Thermo Fisher Scientific, catalog # A37573) following the manufacturer's

10 instructions. All positive hits were re-streaked onto fresh LB-agar plates containing 20

11 µg/mL Cm, 100 µg/mL Tmp, 50 µg/mL Spec, and grown overnight at 37 °C. Individual

12 colonies were grown in liquid culture and subjected to DNA sequencing to confirm the

13 location of glycosites and to protein glycosylation analysis as described below.

14 **Protein isolation.** For Western blot analysis and protein activity assays, cell-free culture

15 supernatants were generated by subjecting 1.5 mL of cells that had been induced for 16

16 h to centrifugation at 13,4000 × g at 4 °C for 2 min. Periplasmic fractions were generated

17 by subjecting 3 mL of 16-h-induced cultures to centrifugation at 13,400 × g for 2 min. The

18 resulting pellets were resuspended in 300 µL of 0.4 M arginine and incubated at 4 °C for

19 1 h with gentle shaking. After centrifugation at 13,400 × g for 2 min, the supernatant

20 containing periplasmic extracts was collected. For stability assays, YebF-Im7, YebF-

21 RNase A, and YebF-scFv-HER2 variants were purified from supernatant fractions and

22 soluble lysate fractions. To prepare the latter, cells expressing YebF-RNase A variants

23 were harvested by centrifugation at 6000 × g at 4 °C for 20 min and the pellets were

24 resuspended in PBS buffer supplemented with 10-mM imidazole followed by cell lysis

25 using a Emulsiflex-C5 Homogenizer (Avestin) at 16,000–18,000 psi. The resulting lysate

26 was clarified by centrifugation at 15,000 × g for 30 min at 4 °C to collect the soluble

27 fraction. All soluble fractions, or supernatant fractions supplemented with 10-mM

28 imidazole, were then applied twice to a gravity flow column loaded with Ni-NTA resin at

29 room temperature and washed with PBS containing 20-mM imidazole until the

30 concentration was lower than 0.1 mg/mL. Proteins were eluted in 2.5 mL of PBS with 250

1   mM imidazole. The eluted proteins were desalted using PD10 Desalting Columns (GE

2   Healthcare) and stored at 4 °C.

3   To produce ColE7 for ELISA experiments, an overnight culture BL21(DE3) cells

4   carrying plasmid pET28a-ColE7 (H569A) was used to inoculate 1 L of LB supplemented

5   with 50 µg/mL kanamycin. Cells were grown at 37 °C until mid-log phase and then were

6   induced with 0.1 mM IPTG for 16 h at 16 °C before being harvested. Following

7   centrifugation at 10,000× g, pellets were resuspended in PBS buffer supplemented with

8   10-mM imidazole and lysed at 16,000–18,000 psi using an Emulsiflex-C5 homogenizer

9   (Avestin). The lysate was clarified by centrifugation at 15,000 × g for 30 min at 4 °C and

10   the collected soluble fraction was mixed with Ni-NTA resin for 2 h at 4 °C. The mixture

11   was then applied to a gravity flow column and washed with 5 column volumes of PBS

12   containing 20 mM imidazole. Proteins were eluted in 4 column volumes of PBS with 250-

13   mM imidazole. The eluted protein was desalted and concentrated to 5 mg/mL in PBS

14   buffer using Ultra Centrifugal Filters with 10-kDa molecular weight cut-off (Amicon®) and

15   stored at 4 °C.

16   **Western blotting analysis.** Supernatant or periplasmic fractions were diluted 3:1 in 4×

17   Laemmli sample buffer (Bio-Rad) and were boiled at 100 °C for 10 min. The treated

18   samples were subjected to SDS-polyacrylamide gel electrophoresis on 10% Mini-

19   PROTEAN® TGX™ Precast Protein Gels (Bio-Rad). The separated protein samples

20   were then transferred to nitrocellulose membranes. Following transfer, the membranes

21   were blocked with 5% milk (w/v) in TBST (TBS, 0.1% Tween 20) and were probed with

22   horseradish peroxidase (HRP) conjugated anti-His antibody (Abcam, catalog # ab1187)

23   or the *C. jejuni* heptasaccharide glycan-specific antiserum hR6 for 1 h. For the latter, goat

24   anti-rabbit IgG (HRP) (Abcam, catalog # ab205718) was used as the secondary antibody

25   to detect hR6 antiserum. After washing three times with TBST for 10 min, the membranes

26   were visualized using a ChemiDoc™ MP Imaging System (Bio-Rad). For all methods

27   related to MS analysis of proteins, see the **Supplementary Methods**.

28   **Cell-free glycosylation.** Methods for purification of *C. jejuni* PglB and isolation of LLOs

29   from glycoengineered *E. coli* were described previously (62). *In vitro*, cell-free

30   glycosylation was carried out in 30-µL reactions containing either 20 µL of supernatant

31   fraction containing aglycosylated YebF-Im7 or 20 µL of periplasmic fraction containing

1   YebF-RNase A, 2 µg of purified *Cj*PglB, and 5 µg extracted LLOs in cell-free glycosylation

2   buffer (10-mM HEPES, pH 7.5, 10-mM MnCl2, and 0.1% (w/v) *n*-dodecyl-β-D-maltoside

3   (DDM)). Reaction mixtures were incubated at 30 °C for 16 h and stopped by adding 10

4   µL of 4× Laemmli sample buffer containing 5% β-mercaptoethanol followed by boiling at

5   100 °C for 15 min, after which they were subjected to Western blot analysis.

6   **ELISA.** Binding activity for Im7 and scFv-HER2 was determined by standard ELISA.

7   Briefly, Costar 96-well ELISA plates (Corning) were coated overnight at 4 °C with 50 µL

8   of 5 µg/mL purified ColE7 in 0.05-M sodium carbonate buffer (pH 9.6) for Im7 variants

9   and 50 µL of 0.2 µg/mL HER2-ED (Sino Biological, catalog # 10004-HCCH) in PBS buffer

10   for scFv-HER2 variants. After blocking with 5% (w/v) non-fat milk in PBS for 1 h at room

11   temperature, the plates were washed three times with PBST (PBS, 0.05% (v/v) Tween-

12   20) and incubated with serially diluted aglycosylated and glycosylated YebF-Im7 and

13   YebF-scFv-HER2 glycovariants for 1 h at room temperature. After washing three times

14   with PBST, 50 µL of 1:2,500-diluted HRP-conjugated anti-DDDK tag antibody (Abcam,

15   catalog # ab49763) for Im7 variants or 50 µL of 1:5,000-diluted HRP-conjugated anti-

16   6×His tag antibody (Abcam, catalog # ab1187) for scFv-HER2 variants, both in 1% PBST,

17   was added to each well for 1 h. Plates were washed three times and then developed using

18   50 µL 1-Step Ultra TMB-ELISA substrate solution (ThermoFisher).

19   **RNase A activity assay**. The enzymatic activity of RNase A variants was assayed using

20   RNaseAlert®-1 Kit (Integrated DNA Technologies) according to the manufacturer's

21   protocol. Each of the 80-times-diluted supernatant samples were normalized to have an

22   OD_{600} equivalent to the positive control strain expressing wt RNase A. Samples were then

23   mixed with 20 pmol of RNase A substrate and 10 µL of 10× RNaseAlert Buffer and

24   incubated in RNase-free black 96 well microplates (Fisher) at 37 °C for 30 min.

25   Fluorescence values were measured at 490 nm/520 nm excitation/emission wavelengths.

26   **Thermal stability analysis.** Far-UV CD spectroscopy of purified Im7 (50-mM sodium

27   phosphate, 400-mM sodium sulfate, pH 7.4) as a function of temperature was carried out

28   in a 0.1-cm cuvette on a spectropolarimeter. Far-UV CD spectra were acquired between

29   200 nm and 260 nm with a step resolution of 1 nm. Melting temperatures of purified

30   glycovariants was determined using high-throughput DSF as previously described (63).

31   Briefly, 5–10 µg of proteins were mixed with Protein Thermal Shift™ Buffer and Protein

1 Thermal Shift™ Dye purchased as Protein Thermal Shift Dye Kit™ (Thermo Fischer

2 Scientific) according to manufacturer's instructions. A melting curve was generated by

3 monitoring fluorescence at 465 nm/610 nm excitation/emission wavelengths while

4 increasing temperature from 10 °C to 90 °C at a rate of 0.06 °C/s on an Applied Biosystem

5 ViiA 7 instrument (Life Technologies). To calculate T_m values, the collected data were

6 analyzed by nonlinear regression analysis using the Boltzmann equation in Prism 8.4.2

7 (GraphPad).

8 **Computational analyses.** For all computational analyses including protein structure

9 preparation, geometric calculations, and Rosetta protocols, see **Supplementary**

10 **Methods**.

11

29

30 **Author Contributions.** M.L. and X.Z. designed and performed all research, analyzed all

31 data, and wrote the paper. S.S., T.J., T.D.M., S.W.H., I.K., J.B., E.C.C., J.W.L., and J.J.G.

1   designed and performed research, and analyzed data. Q.F. and S.Z. performed MS

2   analysis and analyzed MS data. M.P.D. directed research, analyzed data, and wrote the

3   paper.

4

5   **Data availability.** All data generated or analyzed during this study are included in this

6   article (and its supplementary information) or are available from the corresponding

7   authors on reasonable request.

8

9   **Competing Interests**. M.P.D. has a financial interest in Glycobia, Inc., SwiftScale

10 Biologics, Inc., and Versatope Therapeutics, Inc. M.P.D.'s interests are reviewed and

11 managed by Cornell University in accordance with their conflict of interest policies. J.J.G.

12 is an unpaid board member of the Rosetta Commons. Under institutional participation

13 agreements between the University of Washington, acting on behalf of the Rosetta

14 Commons, Johns Hopkins University may be entitled to a portion of revenue received on

15 licensing Rosetta software including some methods developed in this article. As a

16 member of the Scientific Advisory Board, J.J.G. has a financial interest in Cyrus

17 Biotechnology. Cyrus Biotechnology distributes the Rosetta software, which may include

18 methods mentioned in this article. J.J.G.'s arrangements have been reviewed and

19 approved by the Johns Hopkins University in accordance with its conflict of interest

20 policies. All other authors declare no competing interests.

21

22 **References**

23 1.   G. A. Khoury, R. C. Baliban, C. A. Floudas, Proteome-wide post-translational
24   modification statistics: frequency analysis and curation of the swiss-prot database.
25   *Sci Rep* **1** (2011).
26 2.   C. T. Walsh, S. Garneau-Tsodikova, G. J. Gatto, Jr., Protein posttranslational
27   modifications: the chemistry of proteome diversifications. *Angew Chem Int Ed Engl*
28   **44**, 7342-7372 (2005).
29 3.   M. Abu-Qarn, J. Eichler, N. Sharon, Not just for Eukarya anymore: protein
30   glycosylation in Bacteria and Archaea. *Curr Opin Struct Biol* **18**, 544-550 (2008).
31 4.   A. Varki, Biological roles of glycans. *Glycobiology* **27**, 3-49 (2017).
32 5.   N. Mitra, S. Sinha, T. N. Ramya, A. Surolia, N-linked oligosaccharides as outfitters
33   for glycoprotein folding, form and function. *Trends Biochem Sci* **31**, 156-163
34   (2006).

6. F. S. van de Bovenkamp *et al.*, Adaptive antibody diversification through N-linked glycosylation of the immunoglobulin variable region. *Proc Natl Acad Sci U S A* **115**, 1901-1906 (2018).

7. G. T. Beckham *et al.*, Harnessing glycosylation to improve cellulase activity. *Curr Opin Biotechnol* **23**, 338-345 (2012).

8. L. X. Wang, X. Tong, C. Li, J. P. Giddens, T. Li, Glycoengineering of antibodies for modulating functions. *Annu Rev Biochem* **88**, 433-459 (2019).

9. F. Berti, R. Adamo, Antimicrobial glycoconjugate vaccines: an overview of classic and modern approaches for protein modification. *Chem Soc Rev* **47**, 9015-9025 (2018).

10. L. Van Landuyt, C. Lonigro, L. Meuris, N. Callewaert, Customized protein glycosylation to improve biopharmaceutical function and targeting. *Curr Opin Biotechnol* **60**, 17-28 (2019).

11. C. J. Bosques, S. M. Tschampel, R. J. Woods, B. Imperiali, Effects of glycosylation on peptide conformation: a synergistic experimental and computational study. *J Am Chem Soc* **126**, 8421-8425 (2004).

12. D. Shental-Bechor, Y. Levy, Effect of glycosylation on protein folding: a close look at thermodynamic stabilization. *Proc Natl Acad Sci U S A* **105**, 8256-8261 (2008).

13. J. R. Rich, S. G. Withers, Emerging methods for the production of homogeneous human glycoproteins. *Nat Chem Biol* **5**, 206-215 (2009).

14. T. V. Flintegaard *et al.*, N-glycosylation increases the circulatory half-life of human growth hormone. *Endocrinology* **151**, 5326-5336 (2010).

15. N. Ceaglio, M. Etcheverrigaray, R. Kratje, M. Oggero, Novel long-lasting interferon alpha derivatives designed by glycoengineering. *Biochimie* **90**, 437-449 (2008).

16. A. Lusch *et al.*, Development and analysis of alpha 1-antitrypsin neoglycoproteins: the impact of additional N-glycosylation sites on serum half-life. *Mol Pharm* **10**, 2616-2629 (2013).

17. R. Song, D. A. Oren, D. Franco, M. S. Seaman, D. D. Ho, Strategic addition of an N-linked glycan to a monoclonal antibody improves its HIV-1-neutralizing activity. *Nat Biotechnol* **31**, 1047-1052 (2013).

18. T. Buskas, S. Ingale, G. J. Boons, Glycopeptides as versatile tools for glycobiology. *Glycobiology* **16**, 113R-136R (2006).

19. R. J. Payne, C. H. Wong, Advances in chemical ligation strategies for the synthesis of glycopeptides and glycoproteins. *Chem Commun (Camb)* **46**, 21-43 (2010).

20. M. M. Chen *et al.*, Perturbing the folding energy landscape of the bacterial immunity protein Im7 by site-specific N-linked glycosylation. *Proc Natl Acad Sci U S A* **107**, 22528-22533 (2010).

21. A. A. Ollis, S. Zhang, A. C. Fisher, M. P. DeLisa, Engineered oligosaccharyltransferases with greatly relaxed acceptor-site specificity. *Nat Chem Biol* **10**, 816-822 (2014).

22. G. Zhang, S. Brokx, J. H. Weiner, Extracellular accumulation of recombinant proteins fused to the carrier protein YebF in Escherichia coli. *Nat Biotechnol* **24**, 100-104 (2006).

23. T. J. Mansell, C. Guarino, M. P. DeLisa, Engineered genetic selection links in vivo protein folding and stability with asparagine-linked glycosylation. *Biotechnology journal* **8**, 1445-1451 (2013).

24. C. A. Dennis *et al.*, A structural comparison of the colicin immunity proteins Im7 and Im9 gives new insights into the molecular determinants of immunity-protein specificity. *Biochem J* **333 (Pt 1)**, 183-191 (1998).

25. T. P. Ko, C. C. Liao, W. Y. Ku, K. F. Chak, H. S. Yuan, The crystal structure of the DNase domain of colicin E7 in complex with its inhibitor Im7 protein. *Structure* **7**, 91-102 (1999).

26. A. C. Fisher *et al.*, Production of secretory and extracellular N-linked glycoproteins in Escherichia coli. *Appl Environ Microbiol* **77**, 871-881 (2011).

27. L. E. Yates *et al.*, Glyco-recoded Escherichia coli: Recombineering-based genome editing of native polysaccharide biosynthesis gene clusters. *Metab Eng* **53**, 59-68 (2019).

28. M. Wacker *et al.*, N-linked glycosylation in Campylobacter jejuni and its functional transfer into E. coli. *Science* **298**, 1790-1793 (2002).

29. F. Schwarz *et al.*, A combined method for producing homogeneous glycoproteins with eukaryotic N-glycosylation. *Nat Chem Biol* **6**, 264-266 (2010).

30. M. Kanwar, R. C. Wright, A. Date, J. Tullman, M. Ostermeier, Protein switch engineering by domain insertion. *Methods Enzymol* **523**, 369-388 (2013).

31. A. J. Petrescu, A. L. Milac, S. M. Petrescu, R. A. Dwek, M. R. Wormald, Statistical analysis of the protein environment of N-glycosylation sites: implications for occupancy, structure, and folding. *Glycobiology* **14**, 103-114 (2004).

32. J. D. Valderrama-Rincon *et al.*, An engineered eukaryotic protein glycosylation pathway in Escherichia coli. *Nat Chem Biol* **8**, 434-436 (2012).

33. M. Kowarik *et al.*, N-linked glycosylation of folded proteins by the bacterial oligosaccharyltransferase. *Science* **314**, 1148-1150 (2006).

34. J. M. Silverman, B. Imperiali, Bacterial N-glycosylation efficiency Is dependent on the structural context of target sequons. *J Biol Chem* **291**, 22001-22010 (2016).

35. S. M. Juraja *et al.*, Engineering of the Escherichia coli Im7 immunity protein as a loop display scaffold. *Protein Eng Des Sel* **19**, 231-244 (2006).

36. J. J. Lavinder, S. B. Hari, B. J. Sullivan, T. J. Magliery, High-throughput thermal scanning: a general, rapid dye-binding thermal shift screen for protein engineering. *J Am Chem Soc* **131**, 3794-3795 (2009).

37. R. L. Williams, S. M. Greene, A. McPherson, The crystal structure of ribonuclease B at 2.5-A resolution. *J Biol Chem* **262**, 16020-16031 (1987).

38. U. Arnold, R. Ulbrich-Hofmann, Kinetic and thermodynamic thermal stabilities of ribonuclease A and ribonuclease B. *Biochemistry* **36**, 2166-2172 (1997).

39. R. Grafl, K. Lang, H. Vogl, F. X. Schmid, The mechanism of folding of pancreatic ribonucleases is independent of the presence of covalently linked carbohydrate. *J Biol Chem* **262**, 10624-10629 (1987).

40. R. Gupta, S. Brunak, Prediction of glycosylation across the human proteome and the correlation to protein function. *Pac Symp Biocomput*, 310-322 (2002).

41. M. M. Chen, K. J. Glover, B. Imperiali, From peptide to protein: comparative analysis of the substrate specificity of N-linked glycosylation in C. jejuni. *Biochemistry* **46**, 5579-5585 (2007).

42. K. I. Panov *et al.*, Ribonuclease A mutant His119 Asn: the role of histidine in catalysis. *FEBS Lett* **398**, 57-60 (1996).

43. F. S. van de Bovenkamp *et al.*, Variable domain N-linked glycans acquired during antigen-specific immune responses can contribute to immunoglobulin G antibody stability. *Front Immunol* **9**, 740 (2018).

44. J. C. Krause *et al.*, An insertion mutation that distorts antibody binding site architecture enhances function of a human antibody. *mBio* **2**, e00345-00310 (2011).

45. W. Kightlinger *et al.*, Design of glycosylation sites by rapid synthesis and analysis of glycosyltransferases. *Nat Chem Biol* **14**, 627-635 (2018).

46. J. M. Techner *et al.*, High-throughput synthesis and analysis of intact glycoproteins using SAMDI-MS. *Anal Chem* **92**, 1963-1971 (2020).

47. S. B. Whittaker, G. R. Spence, J. Gunter Grossmann, S. E. Radford, G. R. Moore, NMR analysis of the conformational properties of the trapped on-pathway folding intermediate of the bacterial immunity protein Im7. *J Mol Biol* **366**, 1001-1015 (2007).

48. C. Ruiz-Canada, D. J. Kelleher, R. Gilmore, Cotranslational and posttranslational N-glycosylation of polypeptides by distinct mammalian OST isoforms. *Cell* **136**, 272-283 (2009).

49. G. A. Weiss, C. K. Watanabe, A. Zhong, A. Goddard, S. S. Sidhu, Rapid mapping of protein functional epitopes by combinatorial alanine scanning. *Proc Natl Acad Sci U S A* **97**, 8950-8954 (2000).

50. L. M. Gregoret, R. T. Sauer, Additivity of mutant effects assessed by binomial mutagenesis. *Proc Natl Acad Sci U S A* **90**, 4246-4250 (1993).

51. K. L. Morrison, G. A. Weiss, Combinatorial alanine-scanning. *Curr Opin Chem Biol* **5**, 302-307 (2001).

52. P. M. Rudd *et al.*, Glycoforms modify the dynamic stability and functional activity of an enzyme. *Biochemistry* **33**, 17-22 (1994).

53. S. R. Hanson *et al.*, The core trisaccharide of an N-linked glycoprotein intrinsically accelerates folding and enhances stability. *Proc Natl Acad Sci U S A* **106**, 3131-3136 (2009).

54. R. L. Shields *et al.*, Lack of fucose on human IgG1 N-linked oligosaccharide improves binding to human Fcgamma RIII and antibody-dependent cellular toxicity. *J Biol Chem* **277**, 26733-26740 (2002).

55. W. Kightlinger *et al.*, A cell-free biosynthesis platform for modular construction of protein glycosylation pathways. *Nat Commun* **10**, 5404 (2019).

56. A. Natarajan *et al.*, Engineering orthogonal human O-linked glycoprotein biosynthesis in bacteria. *Nat Chem Biol* **16**, 1062-1070 (2020).

57. F. S. van de Bovenkamp, L. Hafkenscheid, T. Rispens, Y. Rombouts, The emerging importance of IgG Fab glycosylation in immunity. *J Immunol* **196**, 1435-1441 (2016).

58. M. F. Feldman *et al.*, Engineering N-linked protein glycosylation with diverse O antigen lipopolysaccharide structures in Escherichia coli. *Proc Natl Acad Sci U S A* **102**, 3016-3021 (2005).

59. A. A. Ollis *et al.*, Substitute sweeteners: diverse bacterial oligosaccharyltransferases with unique N-glycosylation site preferences. *Sci Rep* **5**, 15237 (2015).

60. M. P. Robinson *et al.*, Efficient expression of full-length antibodies in the cytoplasm of engineered bacteria. *Nat Commun* **6**, 8072 (2015).

61. T. Kortemme *et al.*, Computational redesign of protein-protein interaction specificity. *Nat Struct Mol Biol* **11**, 371-379 (2004).

62. T. Jaroentomeechai *et al.*, Single-pot glycoprotein biosynthesis using a cell-free transcription-translation system enriched with glycosylation machinery. *Nat Commun* **9**, 2686 (2018).

63. U. B. Ericsson, B. M. Hallberg, G. T. Detitta, N. Dekker, P. Nordlund, Thermofluor-based high-throughput stability optimization of proteins for structural studies. *Anal Biochem* **357**, 289-298 (2006).